Modeling of Thermodynamic Effects at Micro-nano Scale of Cathode Spots

Bin Xu[1,3](徐斌), Mingda Zhang[1](张明达), Fan Jiang[1*](蒋凡), Cheng Li[2*](李诚), Shujun Chen[1](陈树君)

[1]Engineering Research Center of Advanced Manufacturing Technology for Automotive Components, Ministry of Education, Beijing University of Technology, Beijing 100124, China

[2]State Key Laboratory of Precision Welding & Joining of Materials and Structures, Harbin Institute of Technology, Harbin 150001, China

[3]Jinan Jinqiang Laser & CNC Equipment Co., Ltd., Jinan 250306, China

*Correspondence: jiangfan@bjut.edu.cn(Fan Jiang); licheng@hit.edu.cn(Cheng Li)

Abstract：Cathode spots are fundamental to discharge phenomena, driving material erosion and surface functionalization. However, conventional simulations rely on simplified time-averaged heat sources, failing to resolve the discrete, transient extinction and re-ignition dynamics of micro-spots. In this work, we establish a high-fidelity numerical framework based on the Transiently Random Jump (TRJ) model, which captures dual-scale stochastic spot kinetics by coupling microscopic spatial jittering with macroscopic jump intervals. By integrating these stochastic trajectories into a transient thermo-fluid dynamics framework, the model accurately captures highly localized, pulsed heat fluxes and predicts dynamic peak temperatures exceeding 7000 K. Mechanistic analysis reveals that the pulsed evaporative recoil force inside cathode craters acts as the principal hydrodynamic driver for liquid metal ejection, generating plasma jet velocities above 120 m/s. Experimental validation indicates that the TRJ framework quantitatively predicts complex, overlapping micro-crater morphologies. Furthermore, multi-spot interaction analysis demonstrates that spot clustering induces significant non-linear energy superposition and heightened thermodynamic perturbations compared to dispersed distributions. This work provides an essential theoretical foundation for predicting micro-scale surface morphology evolution and optimizing advanced discharge processes. **[Reviewer #1 Comment 1] [Reviewer #1 Comment 6]**

Keywords: Cathode spots dynamics; Thermo-fluidic coupling; Stochastic random walk; Transient numerical simulation; AC arc welding

PACS: 52.80.Mg; 52.40.Hf; 05.40.Fb; 52.65.Kj; 81.20.Vj

1. Introduction

Cathode spots are a hallmark of high-current-density discharge, serving as a fundamental driver of material ablation, sputtering, and surface functional evolution. Characterized by microscopic high-energy density and high-velocity plasma jetting [1,2], these spots play a pivotal role across diverse technological sectors, including high-voltage vacuum circuit breakers, advanced material processing (e.g., Variable Polarity Plasma Arc (VPPA) welding and electrical discharge machining), and aerospace electric propulsion [3-9]. At the microscopic level, the physical mechanism of cathode spots involves an extreme concentration of current within minute areas, with densities typically reaching 10^8 to 10^11 A/m^2. This intensity triggers the instantaneous vaporization of cathode materials, generating the plasma necessary to sustain the arc discharge [10-14]. However, the intense spatiotemporal evolution of cathode spots presents a significant scientific challenge. Precisely understanding their ignition and sustainment mechanisms—along with the resulting transient heat transfer and melting dynamics—remains a cross-disciplinary hurdle spanning plasma physics, surface engineering, and electrical contact technology.

Studies have demonstrated that the dynamic characteristics of cathode spots are highly nonlinear and stochastic, with an exceptionally ephemeral lifetime typically ranging from 10 to 50 ns [15,16]. Their motion follows a high-frequency sequence of "extinction-reignition-stochastic jumping" events [17]. Mechanistically, the intense evaporative recoil pressure from the high-temperature plasma drives the formation of liquid metal jets. The nanosecond-scale interaction between these jets and the dense cathode plasma subsequently triggers new explosive emission centers at adjacent locations, a process known as reignition [18-20]. Driven by this microscale feedback, the macroscopic trajectories of cathode spots manifest as pronounced random walks, often exhibiting fractal geometry [21]. These spatiotemporal dynamics underscore that the energy and momentum delivery from cathode spots to the material surface is inherently transient and pulsed, rather than continuous or stationary [22,23]. Consequently, high-fidelity microscale modeling of these transient interactions is indispensable. Such modeling establishes the theoretical foundation required to optimize plasma processes and achieve precise manipulation of surface micro-morphology.

Due to current limitations in ultra-high spatiotemporal resolution, experimental investigations of cathode spots remain severely constrained, making numerical simulation the primary methodology in this field. However, existing models face significant physical and numerical challenges in fully capturing transient cathode spot dynamics. On one hand, conventional Magnetohydrodynamic (MHD) models are primarily tailored for macro-scale arc plasma flow and

electromagnetic field transport. Near the cathode active spot region, however, physical gradients vary across sub-micron scales comparable to particle mean free paths, violating continuum fluid assumptions and causing standard MHD formulations to simplify the near-electrode sheath into spatially or temporally smoothed boundary inputs [24–28]. Consequently, macro-scale approaches fail to resolve the discrete, pulsed recoil pressure and micro-crater jetting. On the other hand, while microscale models—such as 2D localized or Smoothed Particle Hydrodynamics (SPH) models—effectively resolve instantaneous mechanisms like individual crater excavation and dual-jet flow [29–33], they overlook the stochastic coupling of successive hopping sequences. Consequently, both approaches lack the ability to model the discrete, pulsed energy and momentum characteristic of nanosecond extinction-reignition sequences along dynamic spatial paths. Bridging this gap requires coupling dynamic stochastic spot trajectories with sub-nanosecond multiphase interface tracking to predict spot-induced metal ejection and microscale surface evolution accurately. **[Reviewer #2 Comment 6]**

To address these limitations, this study presents a high-fidelity numerical framework based on the TRJ model to resolve cathode spot dynamics. To highlight its methodological advances, TRJ is explicitly contrasted with benchmark models—Fixed Heat Source (FHS), Gaussian Random Walk (GRW), and Continuous-Time Gaussian Random Walk (CTGRW)—across three dimensions. Regarding time-scale resolution, FHS enforces continuous heating and GRW/CTGRW lack thermal feedback, whereas TRJ resolves dual-scale kinetics bridging nanosecond jittering with microsecond jumps. For spatial jump characteristics, TRJ replaces stationary or symmetric unconstrained steps with adaptive trajectory mechanics capturing local boundary perturbations. Crucially, in morphology prediction, unlike GRW/CTGRW which track transport probabilities on static substrates without hydrodynamic coupling, TRJ integrates stochastic trajectories with dynamic thermo-fluid flow, enabling accurate quantitative prediction of overlapping micro-crater evolution and multi-spot energy superposition. The remainder of this paper is organized as follows: Section 2 describes the experimental setup and statistical methods used for morphological validation. Section 3 details the TRJ model formulation and the transient coupling methodology; Section 4 presents the simulation results and dynamic mechanistic analysis; and Section 5 concludes the findings of this study. **[Reviewer #1 Comment 1]**

2. Experimental Setup and Materials

The VPPA apparatus (Fig.1) was employed under ambient atmospheric pressure to generate the transient stochastic inputs and morphological data required for validating the TRJ model. The experiments were conducted on 5056 aluminum alloy plates with dimensions of 200×40×6 mm. Key experimental parameters included a current magnitude of 110 A for both the EN and EP phases and an electrode-to-workpiece gap distance of 4 mm. Cathode spot dynamics were captured using a high-speed camera (NAC Memrecam Q1V) equipped with an AF Micro Nikkor 200mm lens at a frame rate of 50,000 fps (and 90,000 fps for EP phase dynamics) with an exposure time of 1.0 μs. To resolve the cathode spots against the intense arc background, a composite optical filtration system was employed, consisting of neutral density (ND) filters, a diffraction grating, and a 640 nm band-pass filter (FWHM = 10 nm). The stochastic input data, such as spot residency time and jump distance, were extracted from these high-speed sequences to provide the physical basis for the Log-Normal and Gaussian parameters within the TRJ model. Surface topography measurements were conducted using a Super-depth-of-field microscope. **[Reviewer #1 Comment 7]**

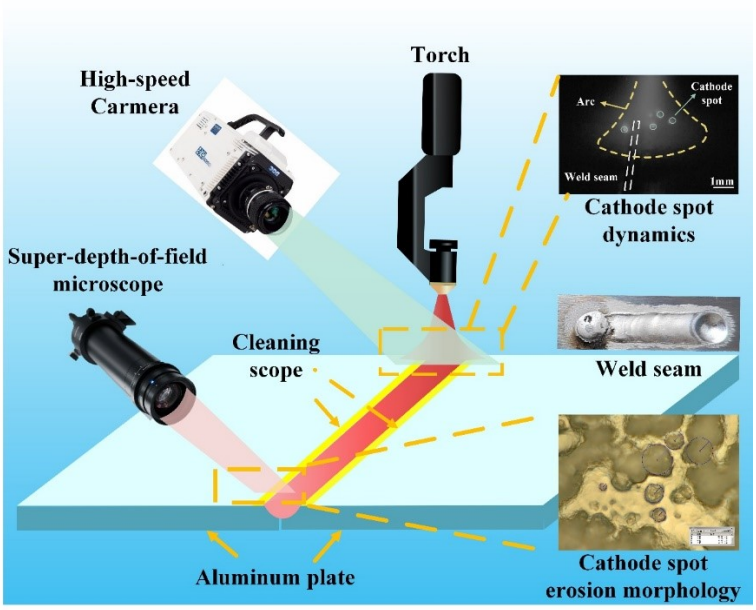


Fig.1 Experimental setup and multi-scale diagnostic framework for TRJ model validation.

3. Computational Model and Methods

3.1 Spatio-temporal Evolution Model of Cathode Spots

Conventional Continuous-Time Generalized Random Walk (CTGRW) models typically simplify cathode spot dynamics to instantaneous jumps, thereby inadequately capturing the distinct physical characteristics of the spot during the two fundamental phases: residence (microscopic drift) and jump (macroscopic re-ignition) events. The dynamics of cathode spots

under high-energy input are characterized by pronounced intermittency and burstiness. This requires a modeling framework capable of capturing the high-frequency transient events as well as the stochastic behavior of rare, long-lived spots.

The TRJ model employs a dual-scale stochastic mechanism to accurately couple the processes of instantaneous transition and continuous drift. Specifically, the model decomposes the cathode spot motion within a Δ t cycle into two independent stages: a macroscopic jump (which models re-ignition at a new location after the extinction of the previous spot) and a microscopic drift (which simulates the subtle oscillations during the spot's residence period).

The residence time (Δ t), which defines the jump interval, is the pivotal temporal parameter in the CTGRW framework. To ensure the model exhibits diffusive behavior and accurately replicates the macroscopic features observed during stable VPPA arc operation, Δ t is constrained to possess a finite mean. Building upon experimental observations and established physical principles, the present model rigorously defines Δ t using the Log-Normal distribution. The Probability Density Function (PDF) of this distribution is defined as:

$$f(\Delta_t;\mu_t,\sigma_t)=\frac{1}{\Delta_t\sigma_t\sqrt{2\pi}}\exp\left(-\frac{(\ln(\Delta_t)-\mu_t)^2}{2\sigma_t^2}\right)\#(1)$$

The selection of the Log-Normal distribution is motivated by its right-skewness and heavy-tailed characteristics [32], statistical properties that are highly congruent with the physical nature of cathode spot behavior. This alignment captures the phenomenon where the majority of spots exhibit extremely short lifetimes (tens of nanoseconds), but rare stochastic events (the heavy tail) yield substantially longer-lived spots—a signature of nonlinear, potentially explosive events in plasma. The model parameters μ t = −17.845 and σ t = 0.5 were directly extracted via statistical fitting of residence times from our high-speed imaging at 50,000 fps. Utilizing the Log-Normal distribution's mean formula, Δ t = exp (μ t + σ t^2/2), the calculated average lifetime (Δ t) is approximately 20 ns. This value demonstrates robust concordance with reported experimental observations of copper cathode spot lifetimes [15,16,34], thereby guaranteeing the physical authenticity of the model's temporal scale from direct experimental observation. **[Reviewer #1 Comment 2]**

Furthermore, the parameter σ t = 0.5 is key in governing the randomness and the depth of the distribution’s tail. This parameter results in a survival time standard deviation (Std/Δ t) of approximately 11.27 ns, leading to a high coefficient of variation (Std/Δ t) of approximately 56%. Physically, this significant volatility accurately reflects the non-Gaussian, highly stochastic nature of cathode spot lifetimes observed in experimental settings. The frequency histogram of this distribution (illustrated in Fig.2(a)) clearly elucidates its right-skewed property, confirming its efficacy as a model for transient impulse input.

During the macroscopic jump phase, the re-ignition location of the spot is governed by a uniform distribution. Subsequently, the model transitions to the microscopic drift phase. To meticulously delineate the spot's micro-oscillations during the Δ t period, Δ t is discretized into N = 10 minor time steps (averaging 2 ns each), where the spot executes microscopic stochastic drift in every step. The microscopic drift distance Δ r adheres to a Normal (Gaussian) distribution, with a fixed standard deviation σ r of 0.4 μm. This microscale spatial drift parameter was directly adapted from literature constraints based on experimental measurements of the spot's peak instantaneous velocity (approximately 200 m/s) [35,36] and scaled according to the internal time discretization scheme. The simulated trajectory presented in Fig. 2(b) demonstrates the TRJ model's capability in decoupling the cathode spot motion into macroscopic jumps (represented by large vertical displacements) and constrained microscopic drift (indicated by minute horizontal fluctuations), thereby furnishing a transient spatial driver for subsequent thermo-hydrodynamic simulations. **[Reviewer #1 Comment 2] [Reviewer #1 Comment 6]**

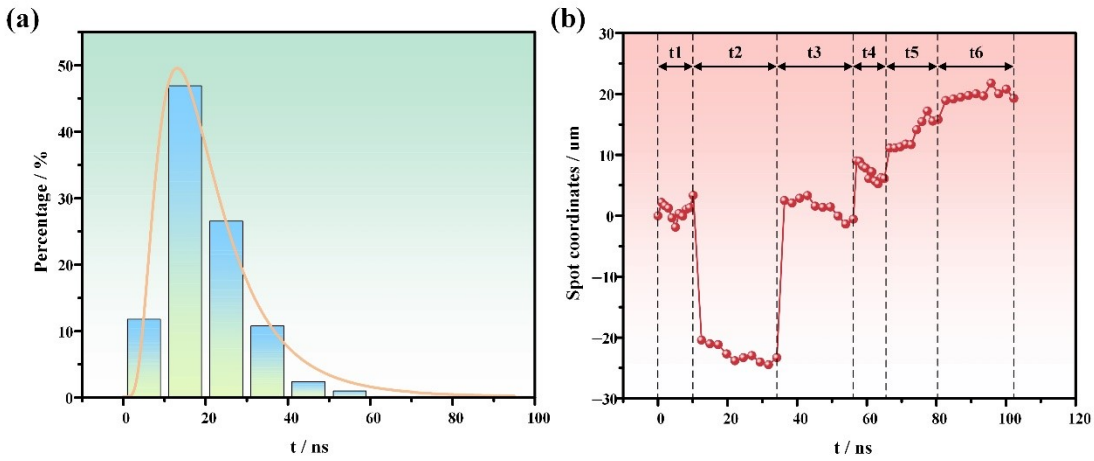


Fig.2: Verification of the Two-Scale Stochastic Mechanism in the TRJ Model: (a) Lognormal probability density function (PDF) and sampling histogram of the residence time (Δ t); (b) Transient random-walk trajectory of the cathode spot on the substrate.

3.2 A Coupled Fluid-Thermal Model for Cathode Spots

The transient two-dimensional framework established in this study analyzes the localized heat transfer and melting dynamics of the VPPA cathode spot. Dynamic trajectories, P(t), generated via custom MATLAB code, were imported into COMSOL Multiphysics (v6.3) to govern the time-dependent center coordinates of heat and momentum inputs. To resolve the dynamic gas-liquid interface during crater excavation and liquid ejection, the Level Set method was employed within the Finite Element framework (FEM), fully coupling the Laminar Flow and Heat Transfer in Fluids physics interfaces with P2+P1 spatial discretization and SUPG/PSPG numerical stabilization. Solution of the monolithic coupled system was executed using a fully coupled Newton-Raphson scheme with the PARDISO direct linear solver leveraging

multi-threaded parallel computation. Time integration was executed via an implicit BDF scheme with a fixed time step of 5×10^{-11} s and a relative solver convergence tolerance of 0.01 across all coupled variables. Local mesh refinement down to 2×10^{-10} m was enforced within the active spot region (verified via grid independence testing) to guarantee solution stability under extreme thermal and momentum pulses. **[Reviewer #2 Comment 1] [Reviewer #2 Comment 4]**

3.2.1 Computational Model and Boundary Conditions

The 70 um×30 um computational domain (Fig.3(a)) covers the molten metal zone under the influence of the cathode spot. This numerical model is based on the crater mechanism (Fig.3(b)), which describes the transient cycle of an existing spot extinguishing, a crater forming, and a new spot stochastically reigniting.

The boundary conditions are defined as follows: the upper boundary (the free gas-liquid surface) accommodates both driving forces (evaporation recoil pressure and Marangoni shear stress) and heat flux dissipation. In contrast, the bottom and lateral boundaries, which constitute the solid-liquid interface, maintain the no-slip condition (v = 0).

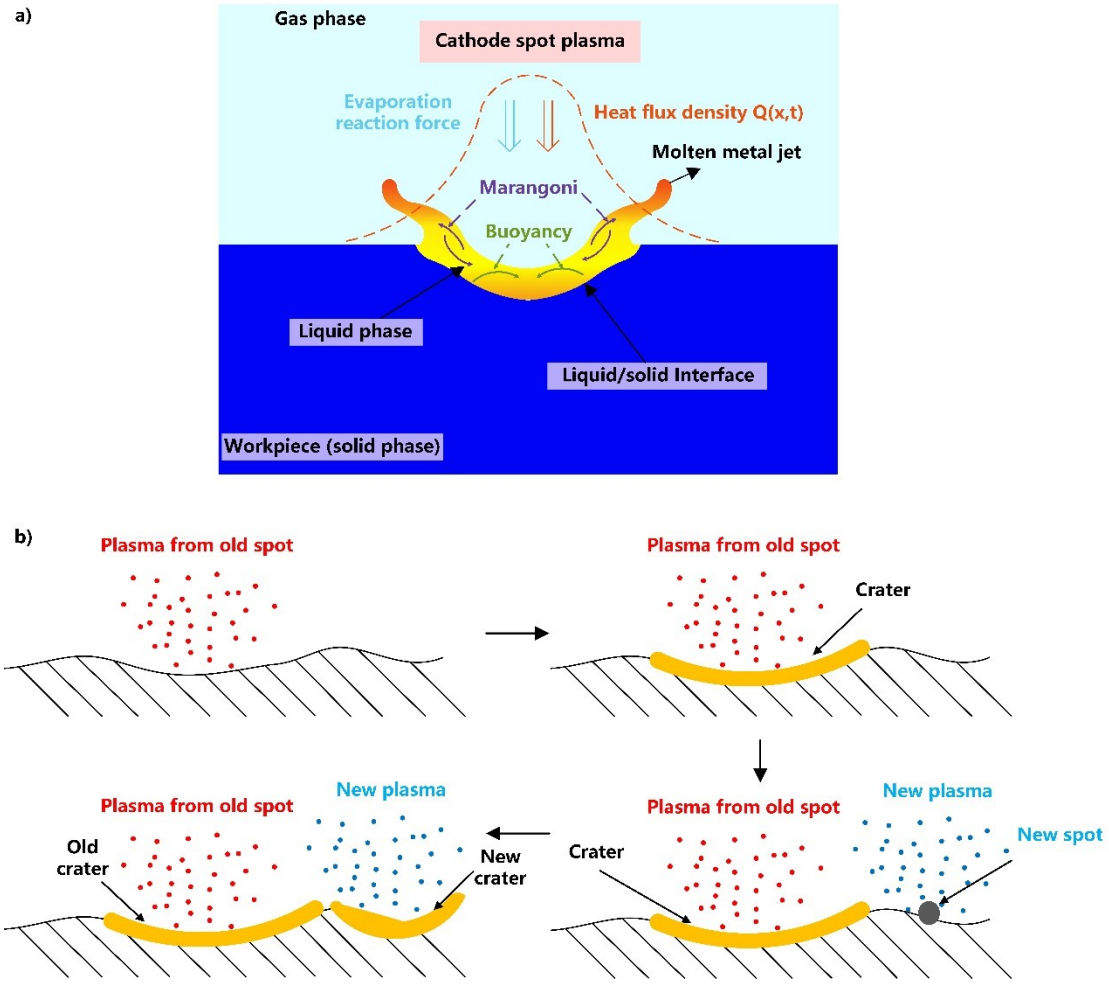


Fig.3 (a) Geometrical and Heat Flux Models for Crater Formation (b) Cathode Spot Evolution

Based on the Crater Model

3.2.2 Momentum Conservation Equation and Pulsed Driving Mechanism

Fluid continuity is governed by the mass conservation equation, while the momentum conservation equation defines the driving forces for fluid flow within the cathode spot crater:

$$\frac{\partial \rho}{\partial t} + \nabla \cdot (\rho v) = 0 \#(2)$$

$$\rho\left[\frac{\partial v}{\partial t} + (v \cdot \nabla)v\right] = -\nabla_P + \nabla \cdot \left[\mu(\nabla_v + (\nabla_v)^T) - \frac{2}{3}\mu(\nabla \cdot v)\right] + \rho g + J \times B$$

$$+P_r \cdot \delta n + \left[-\gamma \kappa n + \frac{\partial \gamma}{\partial T}(\nabla T - (n \cdot \nabla T)n)\right]\delta - A_{mush}\frac{(1-f_l)^2}{f_l^3 + \varepsilon}(v - v_i) \#(3)$$

Where the terms on the right-hand side correspond to the pressure gradient, viscous stress, gravity, electromagnetic Lorentz force, evaporation recoil pressure, surface tension, and Marangoni force induced by the temperature gradient, respectively. Surface tension forces and Marangoni thermocapillary effects are applied along the interface with a baseline surface tension γ_0 = 0.91 N/m and a temperature coefficient dγ/dT = -0.35$\times 10^{-3}$ N/(m*K). To model the solid-liquid phase transition, the enthalpy-porosity formulation governs the Darcy damping sink term (the last term in Eq. (3)), where the liquid fraction fl is defined as a piecewise function of local temperature: **[Reviewer #2 Comment 3]**

$$f_l = \begin{cases} 0, & T \le Ts \\ 1, & T > T_l \\ \dfrac{(T - Ts)}{(Tl - Ts)}, & Ts < T < Tl \end{cases} \#(4)$$

Between the solidus (Ts = 934 K) and liquidus (Tl = 964 K) temperatures. The mushy zone constant is set to A_{mush} = 10^6 kg/(m^3*s) with ε = 0.001 to prevent division by zero, seamlessly driving fluid velocity to zero in solid regions. **[Reviewer #2 Comment 2]**

The primary driving forces in the momentum conservation equation stem from the transient momentum impulse delivered by the cathode spot and localized electromagnetic effects. Specifically, the evaporation recoil pressure acts as the crucial pulse-like momentum source central to the spot's dynamic behavior. Its magnitude is determined by the instantaneous surface temperature within the cathode spot crater (T-surface) and is formulated as:

$$P_r = 0.54P_0 \cdot exp\left(-\lambda/K_b\left(1/T_{surface} - 1/T_v\right)\right) \#(5)$$

where P0 is the ambient pressure, Kb is the Boltzmann constant, λ is the latent heat of vaporization per atom, and Tv is the boiling point of the aluminum alloy.

Concurrently, the Lorentz force, which represents the driving force from the localized current field, is computed by solving the electromagnetic field equations (Eq.6). Given that the TRJ heat source model utilizes a Gaussian spatial distribution (Eq.8), the current lines undergo instantaneous constriction upon re-ignition. This effect localizes the energy and current flux at the new spot, resulting in the Lorentz force exhibiting a highly concentrated and pulsed characteristic, which collectively drives the high-velocity melt jet.

$$\nabla \cdot J = 0;\ J = \sigma E;\ \nabla \times B = \mu_o J \#(6)$$

The liquid metal phase is treated as an incompressible Newtonian fluid within the continuum regime. This assumption is physically justified as the maximum liquid Mach number ($M_{al} \approx$ 0.026, derived from peak melt velocity 120 m/s and speed of sound in liquid aluminum 4600 m/s) is well below the compressibility threshold (Ma = 0.3), and the small Knudsen number (Kn < 0.01) confirms that rarefaction effects are negligible. **[Reviewer #2 Comment 7]**

3.2.3 Energy Conservation Equation and Transient Heat Source Model

The Energy Conservation Equation (Eq.7) is utilized to compute the transient temperature field across the micro-scale domain. The criticality of this equation resides in the precise coupling of the total heat source, Q, which represents the transient thermal input from the cathode spot. Latent heat of fusion (Lf = 3.9×105 J/kg) and latent heat of vaporization (Lv = 7.34×106 J/kg) were coupled into Eq.(7). **[Reviewer #2 Comment 2]**

$$\frac{\partial(\rho c_P T)}{\partial t} + \nabla \cdot (\rho v c_P T) = \nabla \cdot (k \nabla T) - \left[\frac{\partial \rho L}{\partial t} + \nabla \cdot (\rho v L)\right] + Q \#(7)$$

The Total Heat Source (Q) is modeled with a Gaussian distribution. Its peak intensity, Q_1, is calculated using the Joule heating formula (J^2/σ). The TRJ model provides the nanosecond-resolution trajectory sequence, P(t), which is used to define the center of the cathode spot inputs (momentum and heat):

$$Q\ （x,t）= \frac{n \cdot Q_1}{4\pi R^2} exp\left(-\frac{\left(x - P(t)\right)^2}{2R^2}\right) \#(8)$$

R denotes the effective radius of the spot, while P(t) represents the instantaneous positional trajectory generated by the TRJ model.

With respect to the boundary conditions, the aggregate heat flux imposed upon the gas-liquid interface and the metallic side walls of the computational domain encompasses three primary components: convective heat transfer, thermal radiation, and evaporative latent heat loss.

Specifically, the thermal exchange between the molten metal and the ambient environment adheres to the principles of natural convection, wherein the heat transfer coefficient is stipulated as 20 W/(m^2*K). Furthermore, the thermal radiation loss from the metal to the surroundings is governed by the Stefan-Boltzmann law, with the emissivity epsilon meticulously set to 0.4. Initial domain conditions were set to a uniform ambient temperature T_{amb} = 300 K and stationary fluid u = 0. **[Reviewer #2 Comment 5]**

4. Results and Discussion

4.1 Spatio-temporal Analysis of Transient Thermal-Temperature Field Coupling

This section analyzed the transient thermal input and the resulting dynamic temperature response predicted by the TRJ model, elucidating the spatiotemporal coupling of the cathode spot

heat flux. Transient simulations confirmed that the heat flux input was characterized by significant localization and discretization.

Spatially, the heat flux distribution (Fig.4 and 5(a)) followed a characteristic Gaussian morphology. This highly concentrated distribution represented the defining signature of cathode spot activity: the extreme electric field strength at reignition constricted the current, focusing energy into a minute region to form an ultra-high-energy core. This extreme localization served as the necessary precursor for the subsequent initiation of explosive evaporation and the resulting evaporation reaction force pulses.

The temporal profile ((Fig.5(b))) exhibited a pulsed, step-like waveform that reflected the model's "ignition-extinction-transfer" mechanism. During a single cycle, the peak instantaneous heat flux density reached 10^{12} W/m^2 and sustains for approximately 40 ns in the "On" stage. This extreme intensity aligned well with theoretical predictions for cathode spots. The transient spike was primarily caused by the concentrated release of Joule heating (J^2/σ), induced by the extreme current density at reignition. Subsequently, spot transfer or energy balance instability caused the heat flux to rapidly decay, initiating the "Off" state. These observations confirmed that the thermal input of the cathode spot was highly transient and pulsed, rather than continuous or stable.

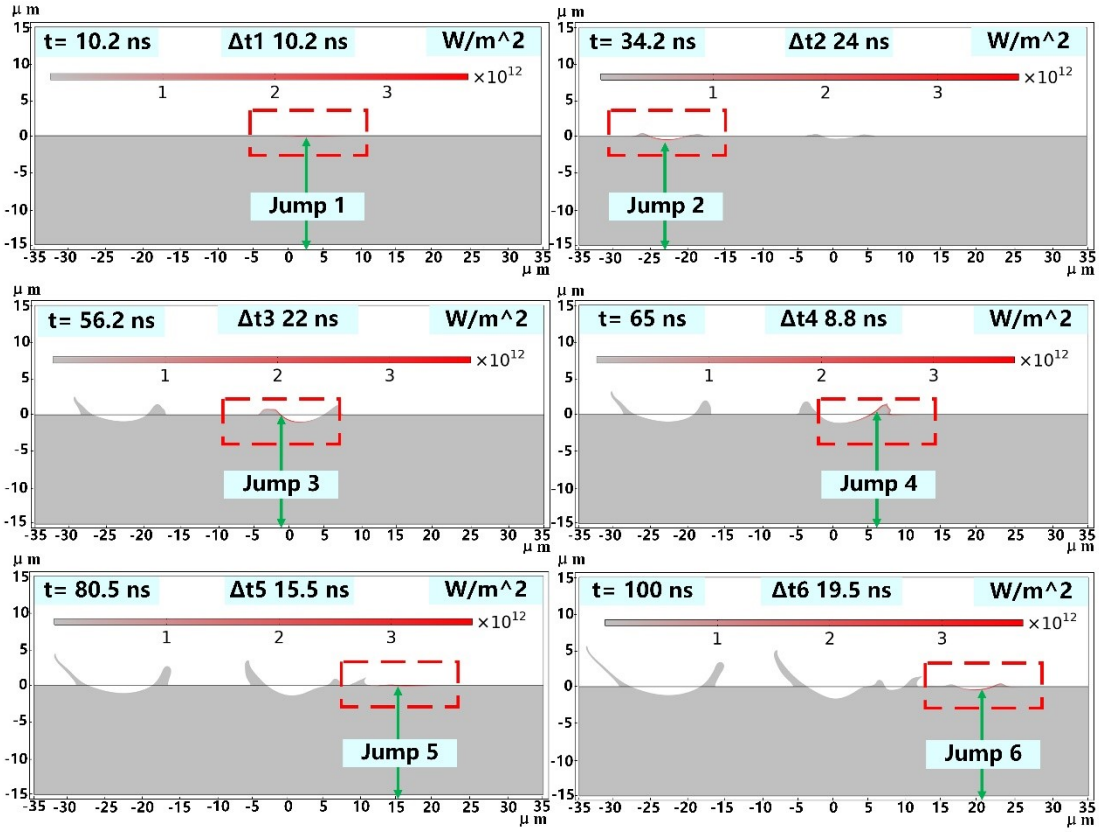


Fig.4 Spatio-temporal evolution of cathode spot heat flux

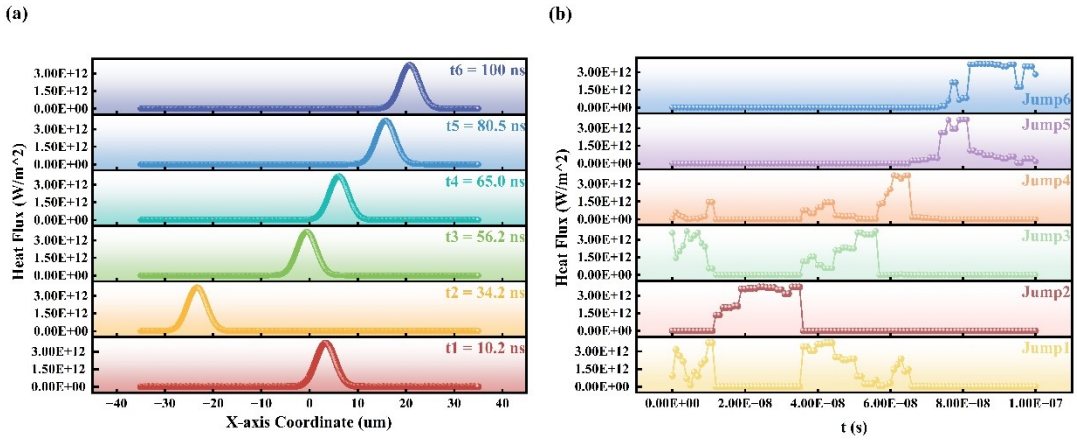


Fig.5 Spatio-temporal characteristics of the transient cathode spot heat flux：(a) The spatial Gaussian profile of surface heat flux at the end of different spot cycles; (b) The pulsed temporal waveform of heat flux at different spot locations (Jump points).

This sudden heat flux spike directly initiates the thermodynamic response, rapidly superheating the local substrate. The impulsive, highly intense thermal energy injection directly established an exceptionally dynamic temperature field on the substrate surface. The instantaneous temperature profiles (Fig.6 and 7(a)) demonstrated that the high-temperature zone matched the heat flux distribution. Crucially, this zone exhibited significant asymmetry as it underwent rapid, nanosecond-scale movement along the TRJ model trajectory. This rapid, asymmetrical movement of the thermal spot provided strong evidence for the TRJ model's dual-scale mechanism: macroscopic stochastic jumping and microscopic localized drift. **[Reviewer #1 Comment 3]**

The temperature history at the central point ((Fig.7(b))) displayed a characteristic sawtooth morphology defined by a rapid ascent and gradual decay. Specifically, during the primary impulse stage (t = 40 ns to 70 ns), the temperature instantaneously peaked at its absolute maximum, exceeding 7000 K. This ultra-fast, nanosecond-scale heating rate signaled the severe transient thermal shock imposed by the cathode spot on the substrate. The asymmetry was highlighted by the steep rise of the heating phase and the relatively shallow slope of the cooling phase. This distinction suggests that while the heating rate within the cathode spot region is driven by the pulsed power (up to 10^{12} W/m^2), the cooling rate is fundamentally limited by thermal diffusion and latent heat dissipation. Because the thermal diffusion timescale vastly exceeded the nanosecond pulse duration, the material was superheated significantly above its boiling point in a minimal interval, which necessitated a much longer period for full thermal energy dissipation. This ultra-rapid heating and delayed cooling cycle served as the principal driver for generating substantial evaporative recoil forces.

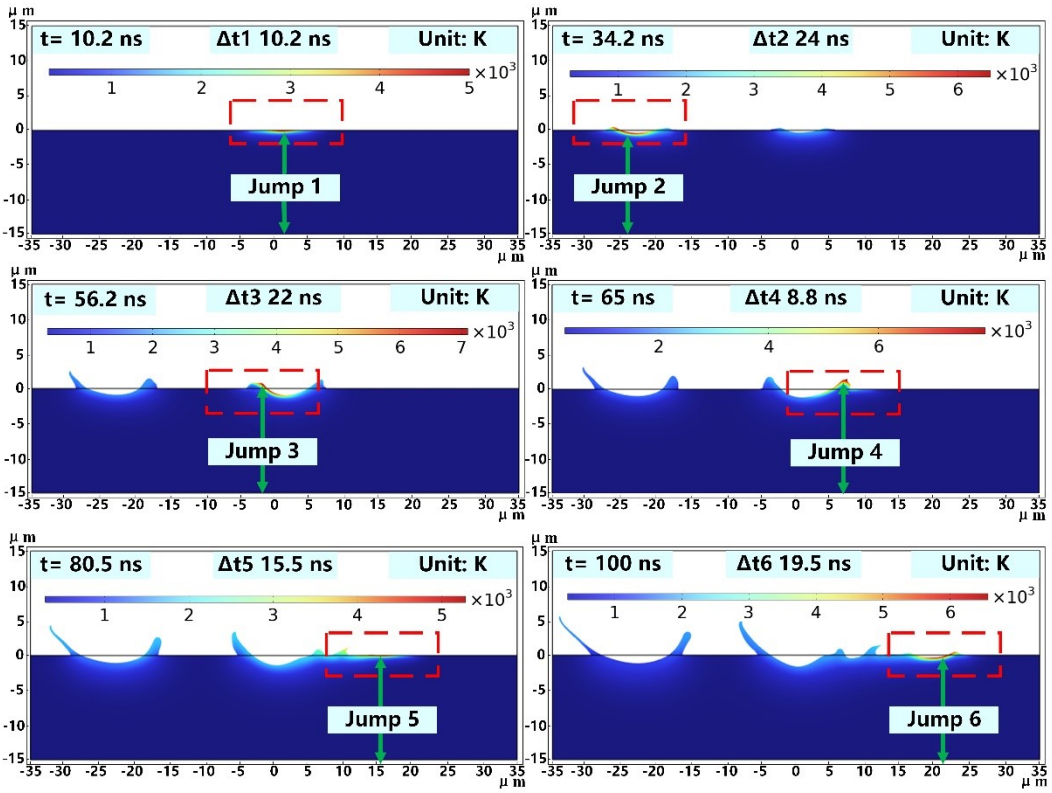


Fig.6 Spatio-temporal evolution of dynamic temperature field

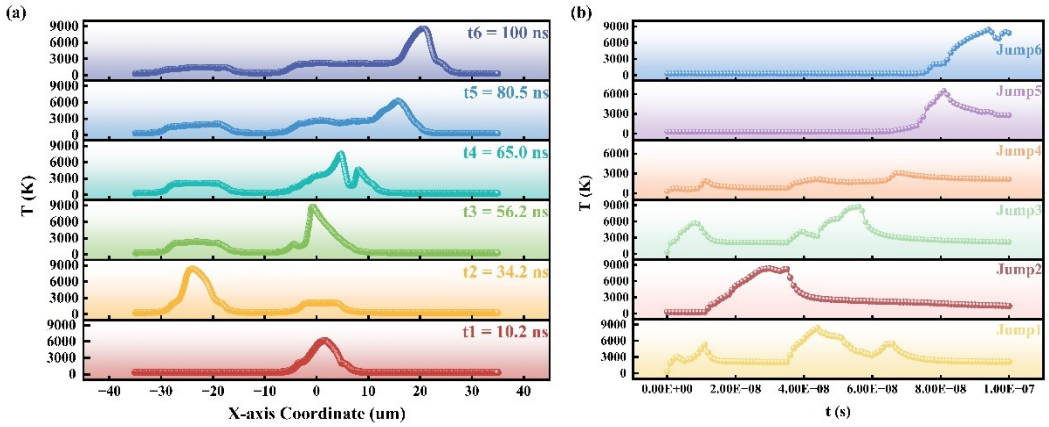


Fig.7 Dynamic temperature response of the substrate: (a) Spatial distribution and (b) Sawtooth temporal profile.

4.2 Transient Momentum Transport and Fluid Dynamics Under Thermo-Hydrodynamic Coupling

As the localized surface temperature peaks beyond 7000 K, intense vaporization is triggered, instantly converting this thermal shock into a mechanical impulse. The evaporative recoil force at the cathode spot serves as the primary driver of momentum transfer to the liquid metal phase. This section explored this transient coupling mechanism and the resulting hydrodynamic response in detail. **[Reviewer #1 Comment 3]**

As illustrated in Fig.8, the characteristics of the evaporative recoil force strongly aligned with

the transient heat flux density features detailed previously.

Spatially (Fig.8(a)), the force profile showed a sharply peaked Gaussian distribution whose maximum precisely coincided with the center of the instantaneous heat flux density. The extreme spatial gradient of this hyper-thermal evaporative force is the critical factor driving the localized fluid within the cathode spot to attain ultra-high instantaneous acceleration.

Temporally (Fig.8(b)), the recoil force exhibited a precipitous pulsed waveform: it instantaneously surged to its peak during the cathode spot's "On" stage and rapidly decayed upon extinction or transfer. The frequency and duration of this mechanical impulse directly mirrored the thermal input characteristics, confirming the efficient and temporal locality of the thermal-to-kinetic energy transfer. This demonstrated the dominant role of the normal force in driving the momentum of the spot-induced melt. **[Reviewer #1 Comment 6]**

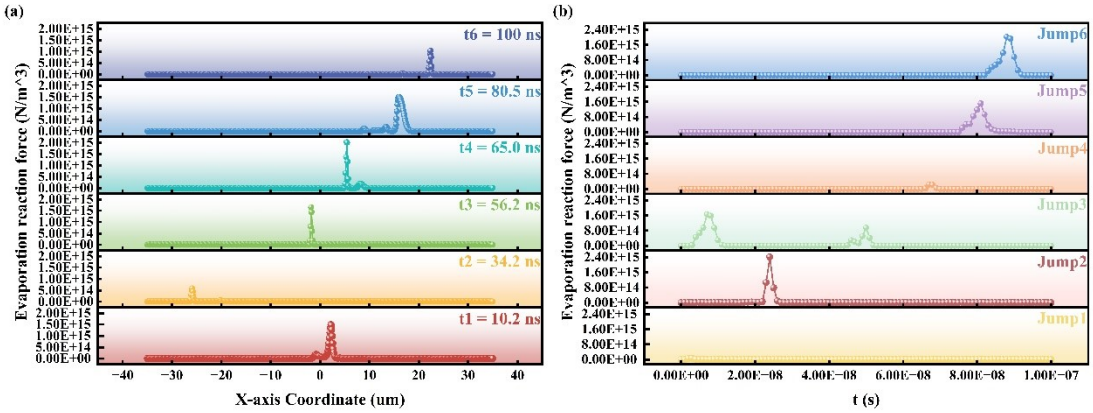


Fig.8 Spatio-temporal characteristics of the transient evaporative recoil force: (a) Spatial distribution of the evaporative recoil force;(b) Pulsed temporal waveform of the recoil force

This localized recoil pressure pulse in turn imparts immediate momentum to the underlying melt pool. The instantaneous fluid velocity map within the cathode spot region, as shown in Fig. 9, substantiates the hypothesis that the local flow is driven by the recoil force. This velocity distribution exhibited extreme spatial localization, with the highest-velocity zone concentrated precisely at the cathode spot's center, manifesting a predominantly radial, outward flow pattern. This demonstrated the absolute dominance of the normal force (i.e., the evaporative recoil pressure) in driving the momentum of the spot-induced melt. Conversely, tangential forces (e.g., the Marangoni effect) played a comparatively secondary role within the core region of the cathode spot. This observation aligned with the findings of Wang et al. [30,33], whose rotating axisymmetric model similarly identified plasma pressure (the evaporative recoil pressure) as the primary motive force for molten metal movement. **[Reviewer #1 Comment 3]**

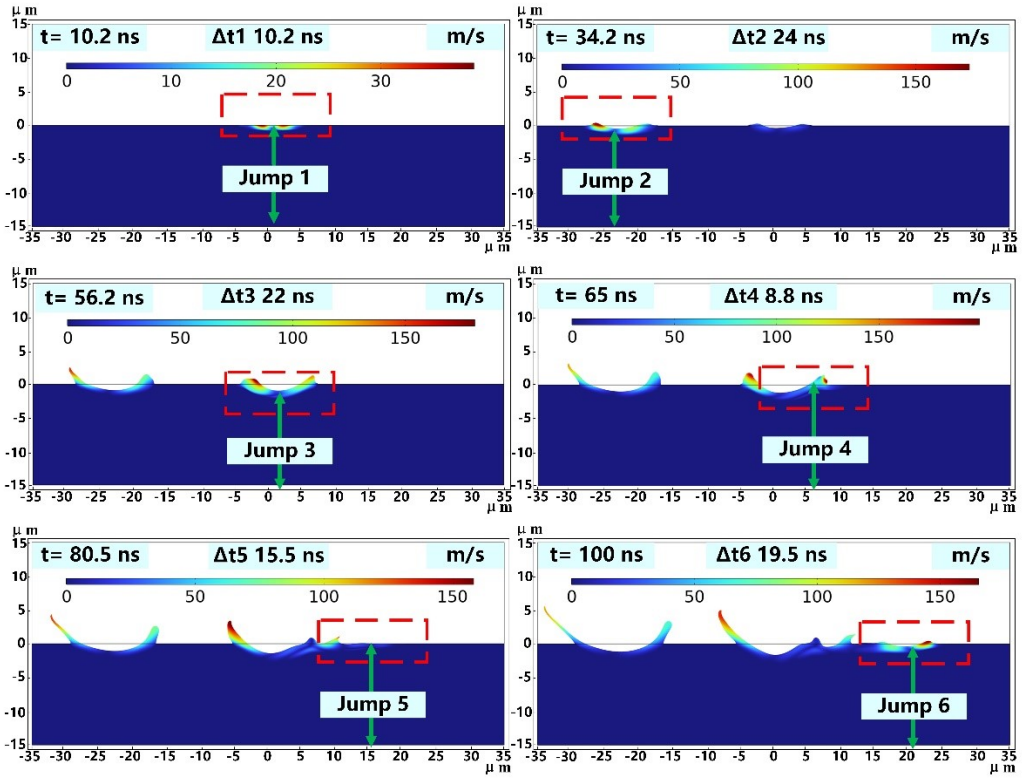


Fig.9 Evaporative recoil force-driven fluid velocity field within the cathode spot crater

The instantaneous spatial distribution of the fluid velocity (Fig.10(a)) was Gaussian-shaped, demonstrating high fidelity to the recoil force distribution (Fig.8(a)). This corroborates the evaporative recoil force as the dominant driver of momentum input at the localized cathode spot. Fig.10(b) further documented the pulse history of the fluid velocity, which was characterized by a steep rising edge and an ultra-high peak velocity of 120 m/s.

A comparative analysis between the pulse of the recoil force (Fig.8(b)) and the fluid velocity (Fig.10(b)) revealed a crucial observation: the peak velocity of the spot-induced melt was precisely synchronized with the maximum evaporative recoil force. This nanosecond-scale temporal synchronicity confirmed the highly efficient and instantaneous conversion of the microscopic thermal pulse into high-velocity momentum. Despite the inherent inertia of the macro-scale molten pool, the brief action timescale (tens of nanoseconds) and extreme thermal flux (10^{12} W/m^2) profoundly accelerated the dynamic response of the localized spot-induced melt.

The observed flow of 120 m/s confirms that the pulsed thermo-mechanical input provides sufficient momentum to overcome the local inertia of the spot-induced melt within this brief duration. This instantaneous, high-velocity fluid motion was the primary cause of rapid micro-crater excavation and material displacement, serving as the key driving force that determined the final microscopic topographical features.

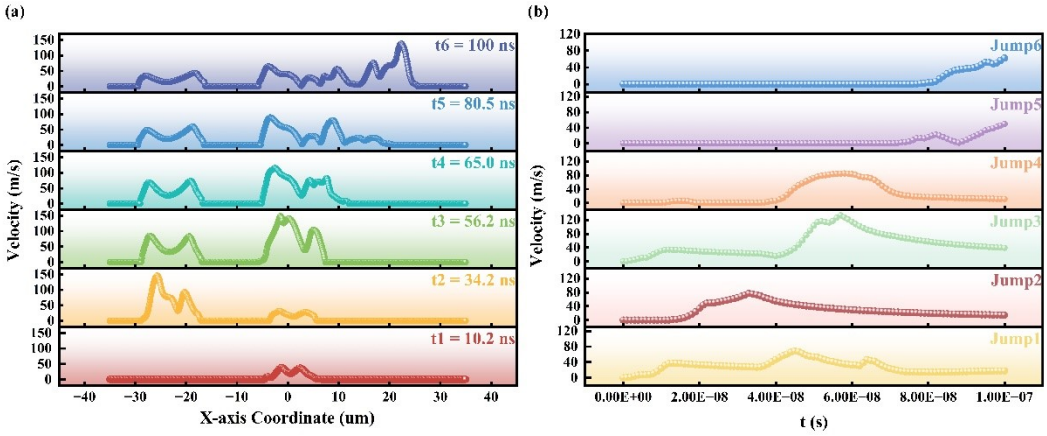


Fig.10 Spatio-temporal evolution of the spot-induced melt velocity: (a) Instantaneous spatial profile of the fluid velocity; (b) Pulsed temporal history of the fluid velocity.

4.3 Micro-morphology Validation

To validate the necessity of the TRJ model in accurately capturing microscopic topographical features, the model's predictions were rigorously compared against those of the conventional Time-Averaged Fixed Heat Source (FHS) model at a current density of J = 7.9×10^{11} A/m^2 (Fig.10).

Experimental observations (Fig.11(a)) on the aluminum cathode surface revealed an array of micro-craters that were non-uniform, varied in size, and exhibited multiple overlapping structures, with radii ranging from 3.4 μm to 6.5 μm. This complex, superimposed morphology was the direct result of the cathode spot's high-frequency, stochastic reignition and jumping behavior. The FHS model, by contrast, failed to replicate these discrete features, further underscoring the critical importance of incorporating spatiotemporal spot dynamics into the numerical framework.

In sharp contrast, the conventional Fictitious Heat Source (FHS) model (Fig.11(b)) predicted only a single micro-crater that was smooth and uniform in size, with a radius of 4.63 μm. This resulting morphology was entirely inconsistent with experimental observations, as it failed to capture the wide variation in crater size and the distinctive overlapping structures. The failure stemmed from the FHS model's reliance on a time-averaged heat source, which severed the physical link between the nanosecond-scale energy pulse input and the spatiotemporal movement of the spot. Consequently, the model lacked the necessary instantaneous momentum input and could not drive the molten metal flow required to form the observed complex crater structures.

Conversely, the morphological features predicted by the TRJ model (Fig. 11(c)) showed good agreement with experimental data, successfully replicating the overlapping and interconnecting structures of multiple spot craters. The predicted crater radii spanned a range from 2.53 μm to 6.82 μm, accurately reflecting the statistical dispersion observed experimentally. This high-fidelity prediction underscored the success of the TRJ model, which was achieved by incorporating

Log-Normal distributed residence times and the Generalized Random Walk (GRW) mechanism. These features allowed the framework to precisely inject energy and momentum into distinct transient locations in a discrete, pulsed manner. This enables the model to capture the dynamic evolution of spot-induced craters under a pulse sequence and the resulting micro-scale morphology. These results further established the necessity of transient coupling in the thermodynamic simulation of cathode spots. **[Reviewer #1 Comment 6]**

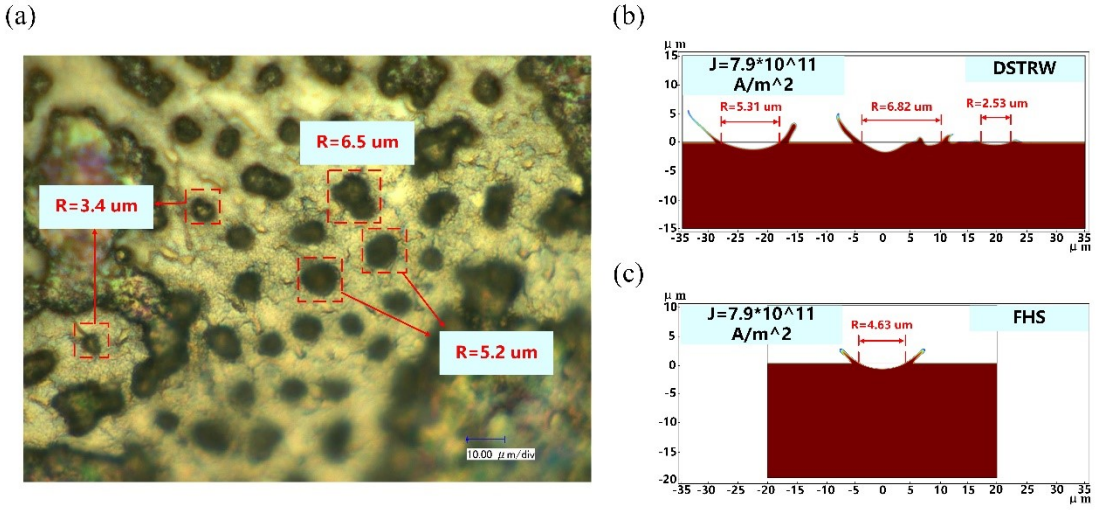


Fig.11 Comparison of micro-crater morphology between experiment and simulation. (a) Experimental observation of the complex, overlapping micro-crater morphology. (b) Prediction of the multiple micro-crater morphology by the TRJ transient coupling model. (c) Prediction of a single, uniform micro-crater by the conventional Time-Averaged Fixed Heat Source (FHS) model.

Having established the necessity of transient coupling, this section validated the TRJ model's predictive accuracy across different operational windows by varying the core process parameter: the cathode spot current density (J). Four representative operating conditions were selected, spanning J values from 4.7×10^{11} A/m^2 to 9.5×10^{11} A/m^2, and the simulated micro-crater morphologies were quantitatively compared with experimental measurements.

Fig. 12 demonstrates that the TRJ model captures the overlapping footprints of the spot-induced melt, confirming the universality of the Log-Normal/GRW mechanism. A positive correlation was observed, where the maximum radius of a single micro-crater, R_max, increased proportionally with the current density (J). For instance, R_max was 3.52 μm at J = 4.7×10^{11} A/m^2, escalating to 9.71 μm at J = 9.5×10^{11} A/m^2. This trend accurately reflected the phenomenon that higher current densities generated stronger instantaneous evaporative recoil forces, which in turn drove the displacement of molten metal over greater distances.

Statistical analysis of the critical micro-crater dimensions across all operating conditions demonstrated that the TRJ model's size prediction error was confined to less than 10%. As the first cathode spot model to verify the transient stochastic input-hydrodynamic coupling, the TRJ framework not only established its innovativeness in numerical simulation but also provided a

reliable and broadly applicable predictive tool for all systems involving high-energy discharge and plasma-material interaction, such as electrical discharge machining, arc deposition, and vacuum switching.

Surface topographies were experimentally characterized using a Super-depth-of-field microscope. Due to the ultra-short residence time of cathode spots, individual micro-craters exhibit shallow depths on the order of ~ 1 μm, where optical vertical measurement incurs significant relative error, preventing direct 3D depth profilometry in the present experimental setup. Nevertheless, quantitative analysis of simulated 3D micro-crater geometry yielded depth-to-diameter aspect ratios (d/D) between 0.14 and 0.22 (predicted crater depths of 0.8 - 1.5 μm and diameters of 6.8 - 13.0 μm). These calculated aspect ratios demonstrate strong quantitative agreement with established numerical simulation models in literature [24,27,30], which similarly report shallow dish-like micro-craters with d/D ~ 0.10 - 0.20 for metallic arc cathode spots. This confirms that the TRJ framework accurately predicts mass displacement in the depth direction. Future work will incorporate high-resolution 3D atomic force microscopy (AFM) to directly measure sub-micron surface topography in the vertical direction. **[Reviewer #2 Comment 9]**

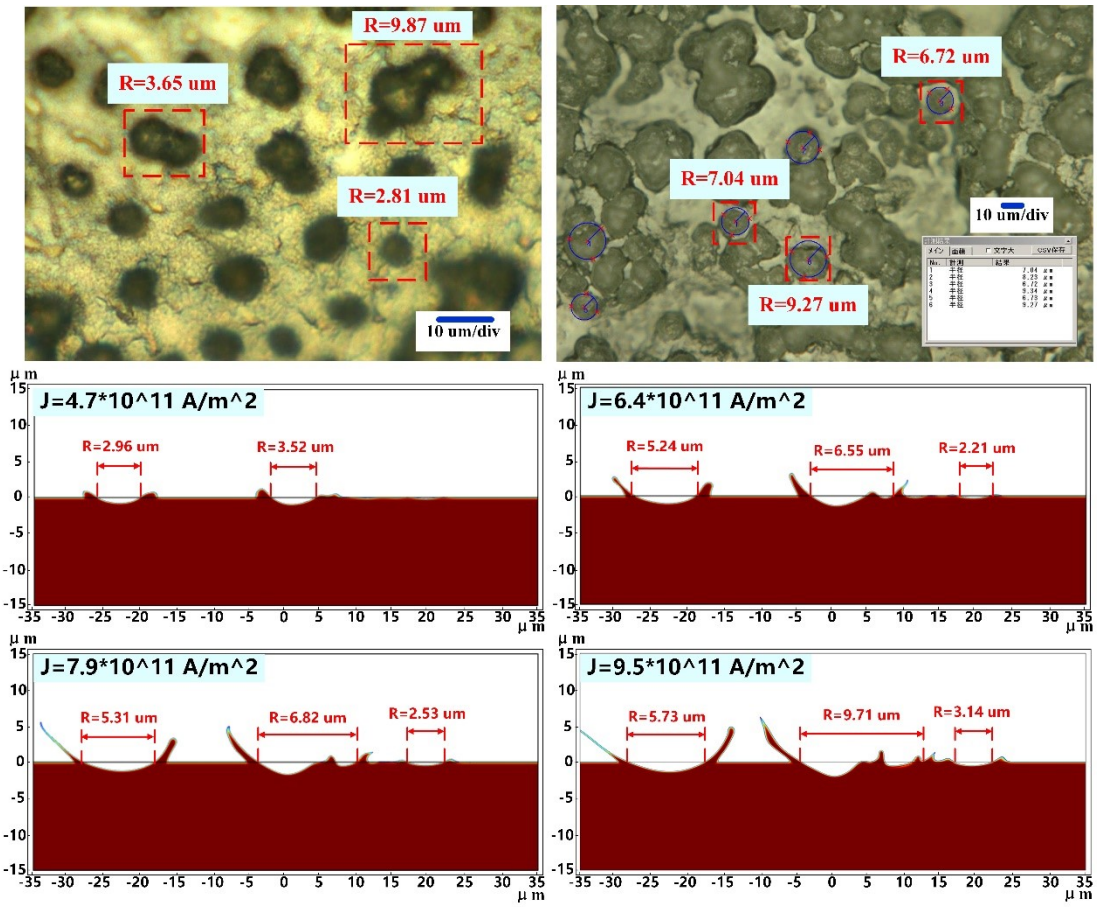


Fig.12 Quantitative validation of TRJ model: Micro-crater morphology prediction across varying current densities.

While post-mortem profilometry validates the final topography, capturing the real-time

excavation dynamics at nanosecond timescales remains an experimental challenge. Future research will incorporate in-situ ultrafast diagnostic techniques to directly capture transient melt jetting and depth evolution. **[Reviewer #2 Comment 8]**

Building upon the validated TRJ model, this investigation delineates the dynamic evolution and reciprocal interaction of spot-induced craters during successive jumping sequences at J = 7.9 $\times 10^{11}$ A/m^2.

As shown in Fig.13, the spot-induced crater transitioned through intermittent stages of heating, lateral displacement, and solidification over the 100 ns simulation period. This evolution was characterized by the cumulative effect of these processes and the resulting reshaping of the surface. In each incremental time step (Δ t), the cathode spot applied thermal shock and momentum at a new, randomly determined location, leading to the rapid ejection and lateral displacement of the molten material. Specific examples of this merging phenomenon were observed at t = 80.5 ns and t = 100 ns, when the newly formed localized melt merged with the boundaries of an existing micro-crater. The subsequent expulsion of molten material accumulated along the periphery, creating irregular, protruding structures that eventually solidified into a complex, asymmetrical topography. This resulting complex structure represented the dynamic origin of the final predicted surface morphology presented in Fig.11(c) and Fig.12.

This kinetic process confirmed the prior conclusion: the complex, overlapping micro-crater structure was not formed by a static heat source, but rather by the random spatial accumulation of multiple nanosecond-scale momentum pulses. Each jump (transposition) of the cathode spot acted as an intense, localized heat source, driving rapid surface evaporation and generating a powerful recoil pressure that ejected the molten metal to form a localized momentum pulse. This random behavior was governed by the GRW mechanism in the TRJ model, which introduced stochasticity to both the timing and location of the spot jumps. Such variability led to differential cooling and solidification rates across the transient micro-craters. The resulting solidified structure exhibited significant dimensional heterogeneity, which was in perfect agreement with experimental observations. The simulated results (Fig.13) demonstrated that the accurate combination of thermal source randomness and fluid dynamics served as the pivotal mechanism for correctly predicting surface erosion in high-energy discharge systems. This finding provided direct theoretical guidance for precisely modulating surface roughness by dynamically controlling the cathode spot's residency time or its spatial jump separation.

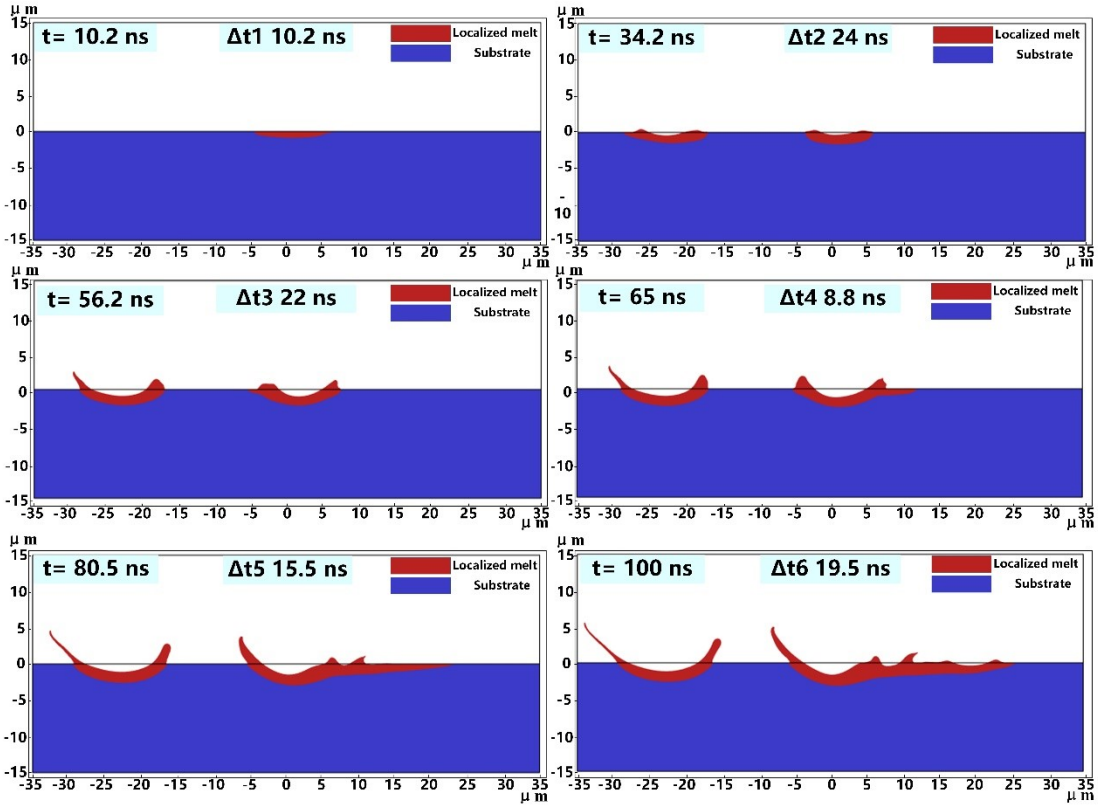


Fig.13 Dynamic evolution of the localized melt profile (Red) under the TRJ model.

4.4 Spatiotemporal Evolution and Thermodynamic Mechanisms of Spots

To accurately replicate the physical environment of the VPPA welding cathode surface, it was essential to investigate how the spatiotemporal distribution of cathode spots influenced the heat transfer and fluid flow within the localized melt.

Observations via the HX-3E high-speed imaging system (sampling at 90,000 fps) revealed the dynamic behavior of cathode spots during the Electrode Positive (EP) phase. As illustrated in Fig. 14, the distribution of these spots at the arc root did not follow a simple, static pattern. Instead, they frequently exhibited two distinct morphological states: "spot clusters," where multiple spots aggregated in a localized area, and "dispersed distributions," where spots maintained significant physical separation.

The comparative analysis across multiple time steps in Fig. 14 confirmed that the transition between cluster and dispersion was not a transient fluctuation but a pervasive physical phenomenon during the welding process. The formation of spot clusters marked a critical shift in energy delivery from individual "point-source perturbations" to "collective heat superposition." This clustering effect was found to induce localized energy oversaturation, profoundly altering the thermal gradient within the localized melt. **[Reviewer #1 Comment 4]**

To systematically analyze the impact of these distribution patterns, the TRJ model was employed to simulate the thermodynamic effects within a 220×110 μm computational domain. Five cathode spots were configured with varying degrees of spatial coupling to represent the transition from dispersed to clustered states, providing a quantitative basis for understanding spot-induced heat flux variations.

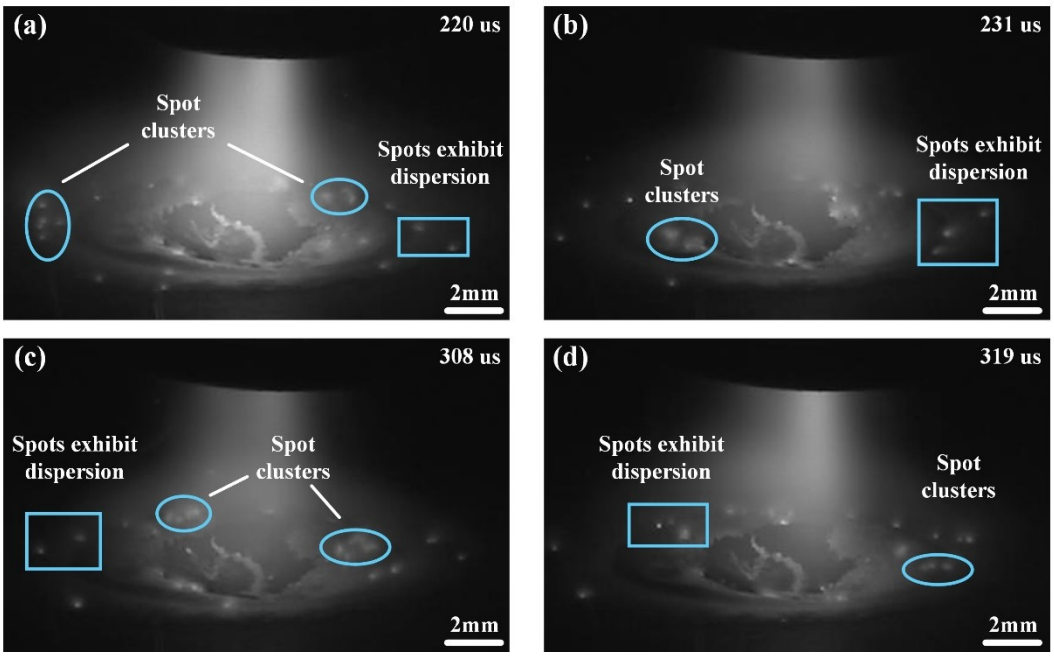


Fig.14 Two typical distribution morphologies of cathode spots in VPPA welding: Clustering and dispersion.

Fig.15 presented a comparison of the transient temperature fields generated by the TRJ model under both spot-cluster and dispersed-distribution modes. In the spot-cluster mode, the frequent ignition, extinction, and overlap of five micro-spots within extremely small spatial and temporal scales resulted in a significant non-linear additive effect of energy input. Simulation data indicated that the instantaneous temperature in the central region was substantially higher than that in the dispersed mode, which led to the formation of a temperature field with an exceptionally high gradient.

Conversely, in the dispersed distribution mode, the thermal loads of the same five spots were effectively "diluted" across the space. Although the heat flux density of an individual spot remained extremely high, the lack of spatial coupling caused the energy field to manifest as multiple, isolated instantaneous hotspots. Consequently, the peak temperature at the center decreased significantly. This comparison revealed that the switching of spot distribution patterns was the fundamental mechanism underlying the large-amplitude fluctuations in heat input on the cathode surface.

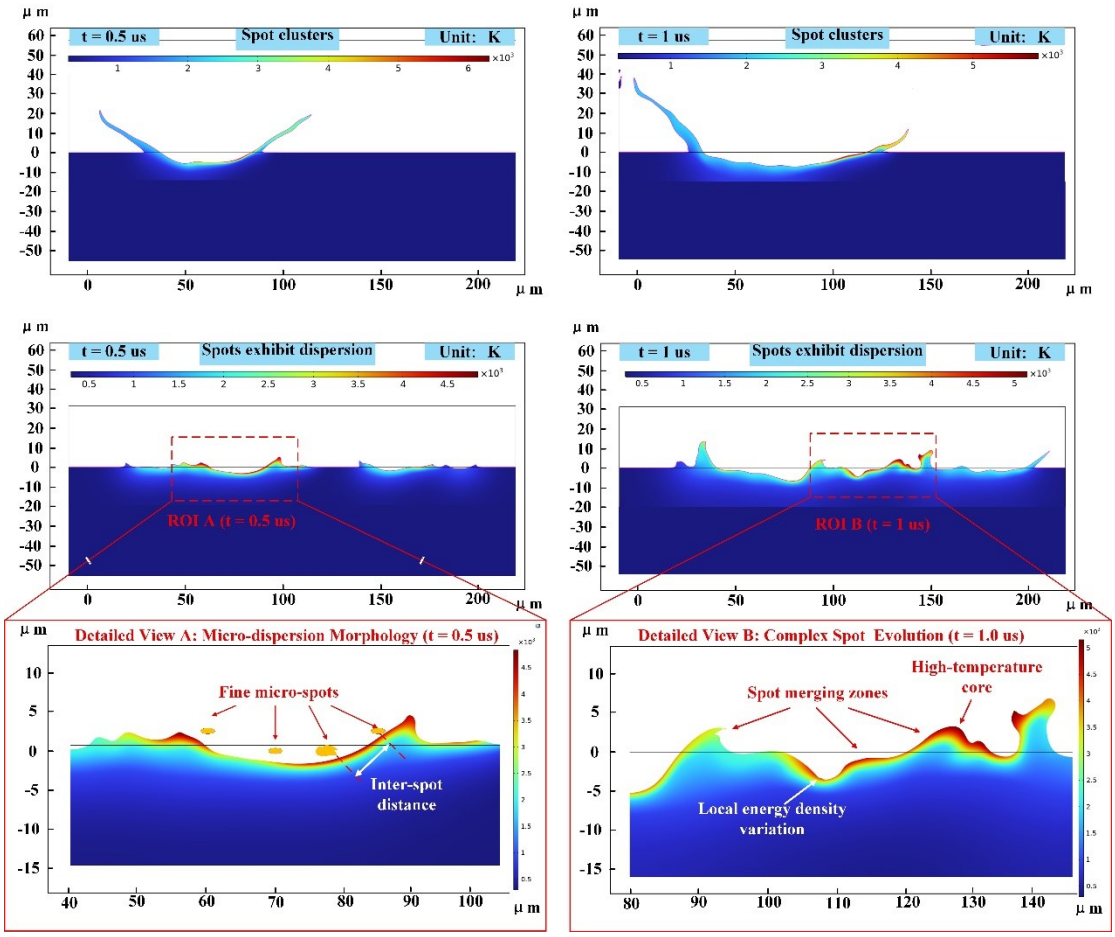


Fig.15 Comparison of transient temperature fields under cathodic spot-cluster and dispersed-distribution modes.

To further examine the dynamic response, Fig. 16 compares the velocity fields driving the localized melt flow under the two distribution modes. In the spot-cluster state, the high-gradient temperature field triggered intense evaporation, which resulted in significant recoil pressure. This pressure produced a powerful momentum transport in the localized area, driving the liquid metal to be violently expelled toward the periphery and forming plasma jets with higher peak velocities.

In contrast, under the dispersed distribution, the velocity field manifested as multi-point, small-amplitude pulse fluctuations. While these fluctuations expanded the high-frequency perturbations on the crater surface, their intensity in driving material migration in the depth direction was notably weaker than that in the spot-cluster mode.

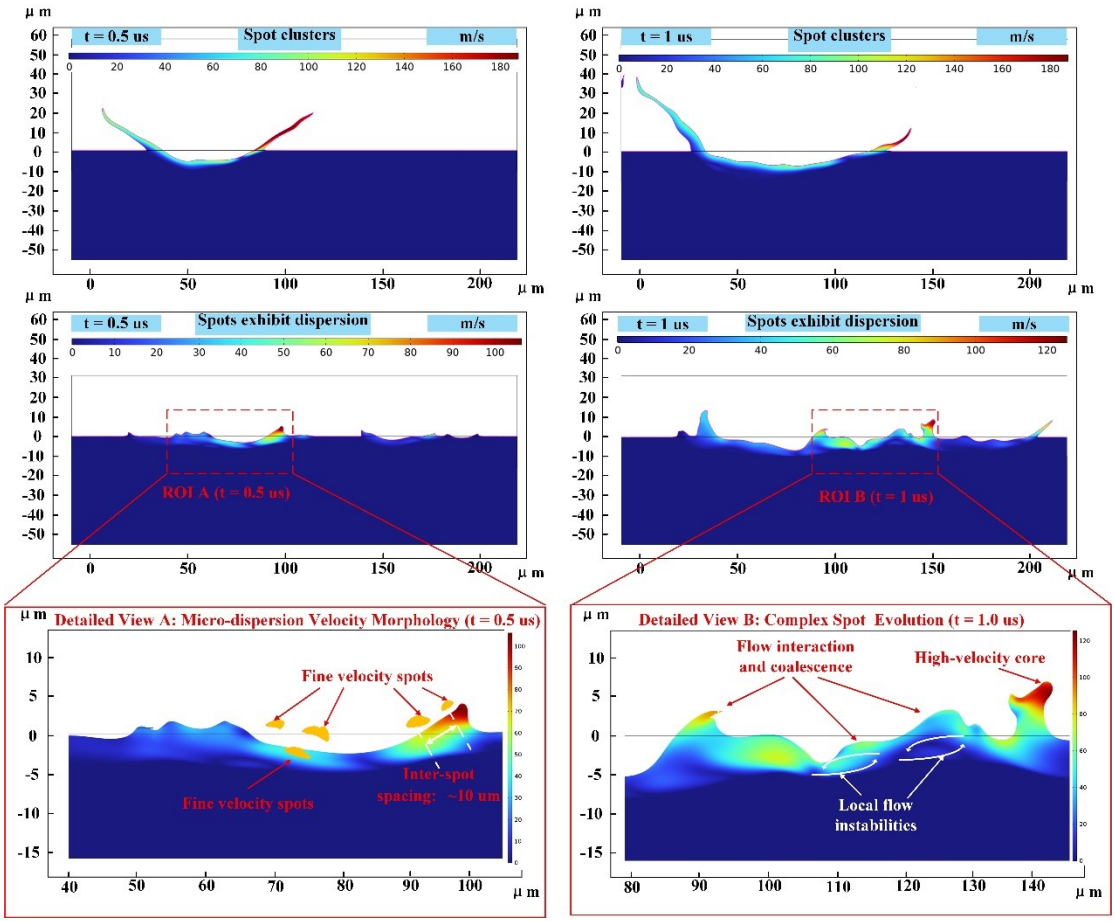


Fig.16 Evolution of localized melt velocity fields under different cathode spot distribution patterns.

Previous studies showed that the spot-induced melt velocity during the EP phase was significantly higher than the fluid velocity observed in the EN phase [7]. Although it was widely speculated that this phenomenon was related to the intense movement of cathodic spots, direct empirical data to verify the contribution of spot perturbations to the velocity field remained scarce due to experimental limitations.

The numerical simulation results in this study provided critical evidence to bridge this gap. It was found that the non-accidental aggregation of spot clusters significantly enhanced the pulse intensity of localized thermal loads. The resulting recoil pressure far exceeded the conventional steady-state arc pressure. This intense thermal-mechanical perturbation, induced by the microscopic clustering of spots, served as the core dynamic factor triggering violent high-frequency oscillations on the liquid metal surface during the EP phase. These findings validate the influence of spot distribution on the spot-induced melt velocity, providing a microscopic basis for the distinct dynamics observed in different VPPA polarity phases.

5.Conclusion

This study established a numerical framework based on the Transiently Random Jump (TRJ) model to overcome the limitations of conventional time-averaged heat source models. By coupling Log-Normal and Gaussian-distributed spot trajectories with a transient thermo-fluidic framework, the model captured the stochastic nature of spot motion and its complex interactions with heat

transfer and fluid flow. This approach enabled the capture of localized, pulsed heat inputs, predicting peak temperatures exceeding 7000 K.

Mechanistic analysis identified the pulsed evaporative recoil force as the main driver of micro-scale fluid flow, generating melt jets exceeding 120 m/s. Comparative simulations revealed that spot clustering triggered significant non-linear energy superposition and heightened thermodynamic perturbations compared to dispersed distributions.

Experimental validation confirmed that the TRJ model predicted the complex, overlapping micro-crater morphologies observed on material surfaces, emphasizing the necessity of modeling spatiotemporal spot dynamics for accurate physical predictions. In summary, this work provides a theoretical foundation for understanding high-frequency energy delivery in discharge systems. **[Reviewer #1 Comment 7]**

Acknowledgement

The authors are grateful to the financial support for this research from the National Natural Science Foundation of China (Grant No. 52375301), National Natural Science Foundation of China (Grant Nos. 52275302 and 52322508), HaiYou Industrial Experts Programme (Grant No. CYLJ20241901412), and Open Project of the Key Laboratory of Multiscale Laser Manufacturing Technology, Ministry of Education.

References

[1] Golizadeh M, Martin F M, Kolozsvari S, Anders A and Franz R 2021 Surf. Coat. Technol. 421 127441

[2] Wu Y, Zhang Y S, Jiang F F, Liu T X, Sun H, Wu Y F, Niu C P, Rong M Z, Luo Z Y and Liu Z Q 2025 J. Phys. D: Appl. Phys. 58 205205

[3] Tsventoukh M M 2021 Phys. Plasmas 28 024501

[4] Zhang M D, Li C, Zheng X F, Xu B, Jiang F and Chen S J 2026 Measurement 271 120813

[5] Ge G W, Liao M F, Duan X Y, Huang Z H, Huang J Q and Zou J Y 2016 Vacuum 134 63

[6] Gohil V and Puri Y M 2017 Proc. Inst. Mech. Eng. B: J. Eng. Manuf. 231 195

[7] Xu B, Zhang C Y, Zhang G K, Jiang F, Tashiro S, Tanaka M and Chen S J 2025 Commun. Mater. 6 94

[8] Zhao Z Q, Pan K, Qi Y L and Sun Q Y 2025 Energy 339 139135

[9] Li Y H, Luo Y, Man C X, Pei X K, Lu X P and Graves D B 2024 Plasma Sources Sci. Technol. 33 105014

[10] Wang C, Shi Z Q, Li W H, Song X C, Jia S L and Wang L J 2015 IEEE Trans. Plasma Sci. 43 2267

[11] Xu P F, Shi Z Q, Guo J, Zhu Q J, Mo Y P, Sun J J and Jia S L 2022 IEEE Trans. Plasma Sci. 50 3742

[12] Benilov M S, Kaufmann H T C, Hartmann W and Benilova L G 2019 IEEE Trans. Plasma Sci. 47 3434

[13] Yang F, Guo Y H, Xue Q G, Zuo H B and Wang J S 2025 Energy 335 138339

[14] Yang J H, Peng C, Ye Z W, Yao C, Zhang X B and Ma Y L 2025 Energy 314 138098

[15] Barengolts S A, Mesyats G A and Shmelev D L 2003 IEEE Trans. Plasma Sci. 31 809

[16] Zhang K, Lang W C, Du H, Chen Z J, Wei X L, Wang X H and Gao B 2023 J. Vac. Sci. Technol. A 41 053001

[17] Liu L M, Yuan Z, Chen L X, Liu S, Ye J J and Jiang W 2022 J. Phys. D: Appl. Phys. 55 475204

[18] Mesyats G A, Bochkarev M B, Petrov A A and Barengolts S A 2014 Appl. Phys. Lett. 104 182109

[19] Shmelev D L, Barengolts S A and Tsventoukh M M 2017 IEEE Trans. Plasma Sci. 45 3046

[20] Sun Q, Yang W and Zhou Q H 2020 J. Phys. D: Appl. Phys. 53 375201

[21] Liang J Y, Oh K, Tsoutas K W, Anders A, McKenzie D R and Bilek M M M 2025 J. Appl. Phys. 138 063301

[22] Beilis I I 2024 Plasma 7 329

[23] Song M M, Liu Z H, Dong Y, Sun Q, Wang Z M, Zhang H T, Wu W B, Yang W and Zhou Q H 2025 Phys. Plasmas 32 023504
[24] Ye J J, Yuan Z, Yang P X, Chen L X, Liu L M, Liu S and Pan Y 2024 IEEE Trans. Plasma Sci. 52 1822
[25] Barengolts S A, Shmelev D L and Uimanov I V 2015 IEEE Trans. Plasma Sci. 43 2236
[26] Qin K, Wang L J, Deng J and Jia S L 2016 Proc. 27th Int. Symp. Discharges and Electrical Insulation in Vacuum (ISDEIV) (Suzhou) p. 1
[27] Kasui D, Nakano Y, Tanaka Y, Ishijima T, Asanuma G, Yamamoto S and Onchi T 2023 Proc. 30th Int. Symp. Discharges and Electrical Insulation in Vacuum (ISDEIV) (Okinawa) p. 221
[28] Kharicha A, Karimi-Sibaki E, Ludwig A and Wu M 2018 Proc. 28th Int. Symp. Discharges and Electrical Insulation in Vacuum (ISDEIV) (Greifswald) p. 467
[29] Mesyats G A and Uimanov I V 2015 IEEE Trans. Plasma Sci. 43 2241
[30] Wang B G, Zhu D H, Ding R, Rohde V, Li C J and Chen J L 2021 Nucl. Mater. Energy 27 100964
[31] Zhang X, Wang L J, Ma J W, Wang Y and Jia S L 2019 J. Phys. D: Appl. Phys. 52 035204
[32] Zhang Y Y, Ma Y, Qiu M X, Liu X H, Deng F P and Jin L J 2024 IEEE Trans. Dielectr. Electr. Insul. 31 738
[33] Ye J J, Yang P X, Yuan Z, Liu L M, Chen L X and Pan Y 2024 AIP Adv. 14 095318
[34] Balanovskii A E 2019 High Temp. 57 8
[35] Tanberg R 1930 Phys. Rev. 35 1080
[36] Phan H L, Tashiro S, Bui V H and Tanaka M 2018 J. Smart Process. 7 243